Structure and Electronic Properties of Hollow-Caged C60 Fullerene-Derived Complexes Introduction

ARTICLE *in* INTERNATIONAL JOURNAL OF QUANTUM CHEMISTRY · JANUARY 2015

Impact Factor: 1.43 · DOI: 10.1002/qua.24840

4 AUTHORS, INCLUDING:

Vladimir Pomogaev
Tomsk State University
26 PUBLICATIONS **79** CITATIONS
SEE PROFILE

Pavel Avramov
Siberian Federal University
92 PUBLICATIONS **522** CITATIONS
SEE PROFILE

Victor Yakovlevich Artyukhov
Tomsk State University
101 PUBLICATIONS **208** CITATIONS
SEE PROFILE

Structure and Electronic Properties of Hollow-Caged C_{60} Fullerene-Derived $(MN_4)_nC_{6(10-n)}$ (M = Zn, Mg, Fe, n = 1−6) Complexes

Vladimir A. Pomogaev,[a] Pavel V. Avramov,*[b] Alex A. Kuzubov,[c,d] and Victor Ya. Artyukhov[a]

Unique hollow-caged $(MN_4)_nC_{6(10-n)}$ (M = Zn, Mg, Fe, n = 1−6) complexes designed by introduction of n porphyrinoid fragments in C_{60} fullerene structure were proposed and the atomic and electronic structures were calculated using LC-DFT MPWB95 and M06 potentials and 6-311G(d)/6-31G(d) basis sets. The complexes were optimized using various symmetric configurations from the highest O_h to the lowest C_1 point groups in different spin states from S = 0 (singlet) to S = 7 (quindectet) for M = Fe to define energetically preferable atomic and electronic structures. Several metastable complexes were determined and the key role of the metal ions in stabilization of the atomic structure of the complexes was revealed. For $Fe_6N_{24}C_{24}$, the minimum energy was reported for C_{2h}, D_{2h}, and D_{4h} symmetry of pentet state S = 2, so the complex can be regarded as unique molecular magnet. It was found that the metal partial density of states determine the nature of HOMO and LUMO levels making the clusters promising catalysts. © 2014 Wiley Periodicals, Inc.

DOI: 10.1002/qua.24840

Introduction

The discovery of fullerene C_{60}[1,2] in 1985 opened a new era in chemistry and material science. $C_{59}B$ and $C_{59}N$ heterofullerene derivatives with carbon atoms substituted by boron and nitrogen, respectively, were synthesized as well.[3,4] A wide variety of exohedral and endohedral C_{60} complexes with metals[5–8] were synthesized experimentally. Nevertheless, until now metal-substituted fullerenes still are neither predicted theoretically nor synthesized experimentally.

Recently, covalent incorporation of Fe-porphyrin-like fragments (FeN_4 moiety) were discovered and elucidated for the carbon nanotubes grown from nanopatterned Fe islands under an NH_3 environment by X-ray and UV PES and *ab initio* Density Functional (DFT) calculations.[9] The authors of Ref. [9] claimed the FeN_4 fragments embedded into carbon environment as "porphyrinoids." In contrast with true metal porphyrins, which consist of central metal ion bound to four pyrrole units, the central Fe ion of "porphyrinoid" fragments[9] are bound to four pyridines. The pyridines form a local structural unit of rhombus symmetry with two distorted pentagons and two distorted hexagons and a Fe ion as a vertex, almost perfectly embedded into graphene lattice. In contrast, four pyrrole units in porphyrins form perfectly flat four distorted hexagons with a metal ion as a vertex.

According to $4n$ + 2 Hückel rule, the aromatic resonance structure of porphyrins consists of 11 double bonds which correspond to 22 π-electrons.[10] In contrast, the π-system of "porphyrinoid fragment"[9] of four pyridines in carbon nanotube consists of 12 double bonds, which perfectly correspond to 24 π-electron antiaromatic system.[11] Nevertheless, the term "porphyrinoid" is not entirely correct in determination of TMN_4 units embedded in sp^2 carbon lattice; it will be used in the text below as it was introduced earlier.[9]

The square and rectangular nanoclusters composed of *meso-meso* β-β fused metalloporphyrins were synthesized experimentally[12–17] as well and supported by DFT and high-level wave function-based electronic structure calculations.[18–21] The 0D and 1D *meso-meso* β-β fused hollow-caged metalloporphyrin nanoclusters were proposed and studied theoretically.[22]

The goal of this article is to design and study the atomic and electronic structures of metal substituted C_{60} $(MN_4)_nC_{6(10-n)}$ (n = 1, 2, 6) nanoclusters formed by introduction of n MN_4 (M = Mg, Fe, Zn) fragments in C_{60} lattice by replacing of n carbon dimers by metal ions and four surrounding carbon atoms by nitrogen ones (Fig. 1). Special attention is paid to analyze the symmetry breaking of the atomic lattices due to correlation effects caused by metal–metal interactions in multiple-substituted nanoclusters. It was found that all $(MN_4)_nC_{6(10-n)}$ nanoclusters are metastable and possess unique atomic structure and electronic properties. For sixfold

[a] *V. A. Pomogaev and Victor Ya. Artyukhov*
Tomsk State University, 36 Lenin Prospekt, Tomsk 634050, Russia
[b] *P. V. Avramov*
Department of Chemistry, Kyungpook National University, 1370 Sankyuk-dong, Buk-gu, Daegu 702-701, Republic of Korea
E-mail: paul.veniaminovich@knu.ac.kr
[c] *A. A. Kuzubov*
Institute of Oil and Gas, Siberian Federal University, 79 Svobodniy Av., Krasnoyarsk 660041, Russia
[d] *A. A. Kuzubov*
Magnetic Phenomena Lab, L.V. Kirensky Institute of Physics SB RAS, Academgorodok, Krasnoyarsk 660036, Russia
Contract grant sponsor: President of the Russian Federation; contract grant number: NSh-1305.2014.2.
Contract grant sponsor: KNU Personal Startup (to P. A.).

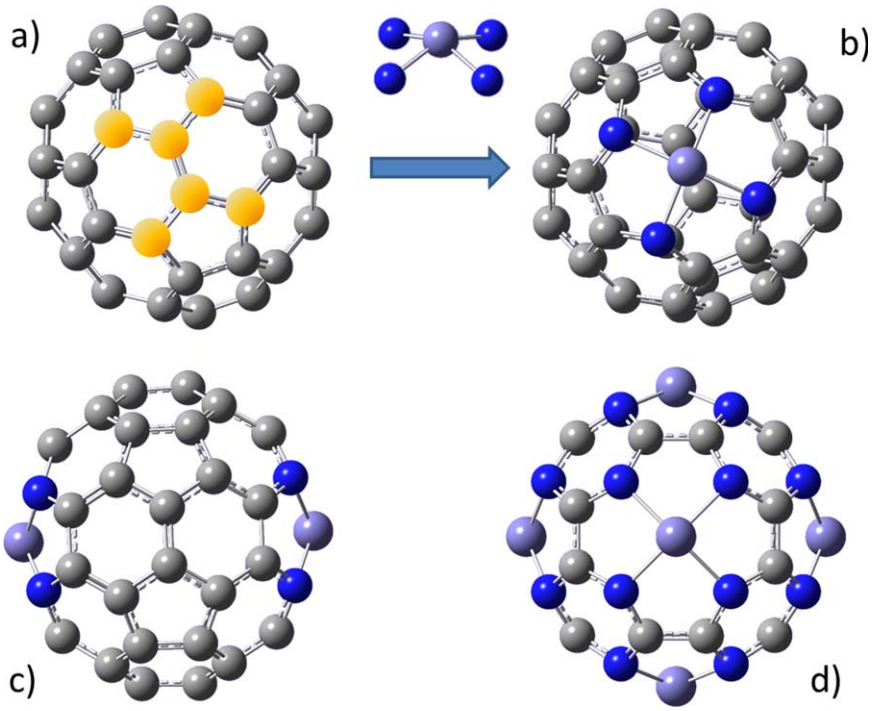

Figure 1. Formation of MN_4C_{54} (b), $M_2N_8C_{48}$ (c), and $M_6N_{24}C_{24}$ (d) (M = Mg, Fe, Zn) nanoclusters from C_{60} (a) by substituting of C_6 fragment (highlighted in yellow) by N_4M fragment (top center of the figure). Carbon atoms are presented in light gray and yellow, nitrogen atoms are presented in blue, metal ion is presented in light blue.

iron-based nanoclusters, the metal–metal interactions play the main role in determination of the spin states and symmetry of the low-energy configurations. The complexes may be highly promising as molecular supermagnets for future nanoelectronic and nanospintronic devices and heterogenic catalysis.

Computational Details and Methodology

Design of the $(MN_4)_nC_{6(10-n)}$ nanoclusters

C_{60} consists of 12 pentagons and 20 hexagons (Fig. 1a). Each single hexagon is connected with three pentagons and three hexagons through carbon dimers with single (pentagon–hexagon) or double (hexagon–hexagon) chemical bonds between the atoms. Substitution of double-bonded C_2 dimer and adjacent four carbon atoms by a MN_4 porphyrinoid unit (Fig. 1b, as previously done[9] for carbon nanotubes) results in novel hollow-cage 0D nanoclusters with metal ions embedded into the carbon wall of parent C_{60}, which affords ample opportunity to control the electronic structure of the molecules by tuning the metal–metal interactions. The icosahedral C_{60} lattice allows one to introduce up to six porphyrinoid fragments by substituting six carbon dimers to form $M_6N_{24}C_{24}$ hollow-cage nanoclusters. The $n = 1$, 2, and 6 cases are presented in Figures 1b–1d, respectively. For $n = 6$ case ($M_6N_{24}C_{24}$ nanocluster, Fig. 1d), all available six dimers are substituted, keeping the high symmetry (O_h point group) of the nanocluster. In this case, each single carbon hexagon is connected with three carbon hexagons and three pentagonal C_4N pyrrole fragments, similar to each single carbon hexagon of C_{60}. For $n = 1$ (Fig. 1b, MN_4C_{54} nanocluster), only one dimer is substituted, keeping the main structural features of C_{60} intact. A double substituted molecule $M_2N_8C_{48}$ (Fig. 1c) is formed in the same manner by substitution of two opposite C_2 dimers. It was found that single- and double-substituted clusters obey the highest C_{2h} point symmetry, while for $Fe_6N_{24}C_{24}$ nanoclusters the correlation effects lead to high-spin states of lower symmetry of C_{2h}, D_{2h}, and D_{4h} point groups.

To elucidate of the role of aromaticity in proposed nanoclusters, a single structural unit of four pyridines, connected with Mg ion, $MgN_4C_{20}H_{12}$, was optimized without symmetry restrictions (Supporting Information Fig. S1). As the resonance structure of $MgN_4C_{20}H_{12}$ consists of 10 double bonds or 20 π-electrons, it obeys $4n$ antiaromatic rule[11] and inclines for structural distortions to decrease the energy. It was found that antiaromaticity of the structural unit leads to departure of the $MgN_4C_{20}H_{12}$ from ideal plain structure to square pyramid with 126° N—Mg—N. The significant distortion of the initial 2D square leads to considerable energetic stabilization of the proposed nanoclusters.

Methods of electronic structure calculations

The DFT approach is extensively used to study the atomic and electronic structure of porphyrin-based nanoclusters.[9,18–23] The long-range corrected (LC) unrestricted DFT potentials of M06[23,24] and MPWB95[25,26] combined with localized basis sets (6-31G(d) on carbon and nitrogen atoms and 6-311G(d) on Mg, Fe, and Zn atoms) implemented in the Gaussian09[27] code were used for accurate reproduction of the atomic and electronic structure of the $(MN_4)_nC_{6(10-n)}$ nanoclusters. Series of works successfully used the single configuration approach

Table 1. Relative energies (kcal/mol) of $Fe_6N_{24}C_{24}$, $Zn_6N_{24}C_{24}$, and $Mg_6N_{24}C_{24}$ nanoclusters in different spin states and symmetries calculated using the MPWB95 potentials for all the compounds and additionally M06 functional for only $Fe_6N_{24}C_{24}$.

Spin states		$Fe_6N_{24}C_{24}$, MPWB95				$Fe_6N_{24}C_{24}$, M06		$Zn_6N_{24}C_{24}$	$Mg_6N_{24}C_{24}$
Multiplicity	Spin	C_{2h}	D_{2h}	D_{4h}	O_h	D_{4h}	O_h	O_h	O_h
Singlet	0	–	37.5	37.5	41.4	58.2	49.2	0	0
Triplet	I	12.2	–	12.2	12.9	12.1	12.9	151.7	133.9
Pentet	II	0.001	0.000	0	3.1	0	3.0		
Septet	III	–	4.1	–	7.6	–	6.2		
Nonet	IV	4.2	–	4.2	5.9				
Undectet	V	0.6	–	0.6	4.5				
Tredectet	VI	–	–	–	6.3				
Quindectet	VII	–	–	–	14.5				

with competitive functionals and basis sets to calculate atomic and electronic structure of C_{60} endohedral complexes with different metals,[22,23,27–34] particularly iron.[22,23,29–31] Authors of Ref. [21] especially emphasized that almost all of the hybrid functionals accurately reproduce the experimental ground spin states of the investigated Fe-porphyrins. The LC DFT potentials provide correct description of the atomic and electronic structure of extended nanoclusters allowing one to take into account weak dispersion interactions.

Formation energies of the nanoclusters were calculated using the following expression:

$$\Delta E = \left(E\left((MN_4)_nC_{6(10-n)}\right) + 3nE(C_2) - E(C_{60}) - 2nE(N_2) - nE(M)\right)/N_{atm},$$

where N_{atm} is a number of atoms in a $(MN_4)_nC_{6(10\ -\ n)}$ nanocluster and E corresponds to total energies of the reactants (C_{60}, N_2, and metal atoms) and products ($(MN_4)_nC_{6(10\ -\ n)}$ and C_2). To calculate the formation energies of all presented nanoclusters, the counterpoise method of Boys and Bernardi[35] was used to correct basis set superposition errors (BSSE). The total and partial electron densities of states were generated by GaussSum code[36] using the corresponding orbital energies and occupancies and the energy smearing factor of 0.2 eV.

Results and Discussion

The relative energies of $M_6N_{24}C_{24}$ (M = Mg, Fe, Zn) nanoclusters (Fig. 1d) in different spin states and symmetries calculated at MPWB95 and M06 DFT levels of theory are presented in Table 1. The frequency analysis does not show an imaginary mode in vibrational spectra (see data in Supporting Information). As the iron-based hollow-caged nanoclusters display very high spin states,[22] all possible spin states of $(FeN_4)_nC_{6(10\ -\ n)}$ clusters should be considered. One can see the most energetically unfavorable spin state is singlet which is significantly higher than the pentet global minimum almost by 40 kcal/mol. The pentet multiplicity of D_{4h} symmetry provides the ground state of $Fe_6N_{24}C_{24}$ nanocluster with vanishing energy differences (less than 0.001 kcal/mol) between D_{2h} and C_{2h} configurations (Table 1). It is worth to note that the energy difference is much smaller than the accuracy of DFT method (~1 kcal/mol).[22–25] This fact makes spin states of the conformers to be competitive and even equivalent in energy. Significant decrease of the total energy by the lowering of the symmetry from O_h point group to D_{4h}, D_{2h}, and C_{2h} point groups display the key role of the electronic correlations caused by open electronic shells in determining the structure and electronic properties of Fe-based hollow-caged structures. Both $Mg_6N_{24}C_{24}$ and $Zn_6N_{24}C_{24}$ molecules are in singlet spin states with triplet states much higher in energy (132 and 152 kcal/mol, respectively, Table 1). Hereafter, $Fe_6N_{24}C_{24}$, $Fe_2N_8C_{48}$, and FeN_4C_{54} are in pentet states, whereas triplet state of single substituted molecule is denoted as FeN_4C_{54} ($S = 1$). Structures higher than quindectet are not discussed in this text because of their very high relative energies.

Optimization of a single $MgN_4C_{20}H_{12}$ structural unit reveals significant distortion of the fragment due to its structural stress and antiaromaticity of the π-system. As it was described earlier in Design of the $(MN_4)_nC_{6(10\ -\ n)}$ nanoclusters section, the $MgN_4C_{20}H_{12}$ cluster is formed by four pyridines and its resonance structure has 10 double bonds or 20 π-electrons which obey $4n$ antiaromatic rule. Electronic factors and structural stress lead to significant bending of the $MgN_4C_{20}H_{12}$ nanocluster with departure from perfect planar N—Mg—N angles from 180° up to 126°. This effect leads to decreasing structural stress and stabilization of closed-shell nanoclusters.

The nature of chemical bonding of nanoclusters in this study is elucidated by analyzing the partial density of states (Fig. 2). For the $Fe_6N_{24}C_{24}$, the carbon p-atomic orbitals (AOs) $|p_C\rangle$ makes significant contribution to α highest occupied molecular orbital (HOMO), H-1, and all vacant molecular orbitals (MOs) (38–65%), as well as for β-MOs from H-4 through L+4 (46–71%). A similar picture is observed for nitrogen p-AOs $|p_N\rangle$ which is complementary to the carbon contribution for α H-1 through L+4 MOs as well as for β H-4 through L+1 ones (Table 2). Significant (31 and 33%) admixture of iron-AOs $|d_{Fe}\rangle$ to $|p_N\rangle$ states (53–55%) in α-MOs of H-2, H-3, and H-4 against the vanishing iron participation in β-MOs of H-2, H-3, and H-4 (4%) was detected (Table 2). Conversely, the $|d_{Fe}\rangle$ is responsible for 20% population of β-L+3, β-L+4, and visible contribution to β-L+2 (12%) orbitals. Thus, spin-polarization appears because of the strong difference between contributions of carbon and nitrogen p-AOs as well as iron d-AOs. The β HOMO → lowest unoccupied molecular orbital (LUMO) splitting $\Delta E_{\beta \to \beta}$ is equal to 2.11 eV (Fig. 2d) that is energetically narrower than $\Delta E_{\alpha \to \alpha} = 2.27$ eV and the $E(\beta\text{-HOMO}) = -4.79$ eV is higher than $E(\alpha\text{-HOMO}) = -5.07$ eV.

The relative energies of different spin states and symmetries of the FeN_4C_{54} nanocluster were calculated, and it was found that maximal singlet-triplet splitting is equal to

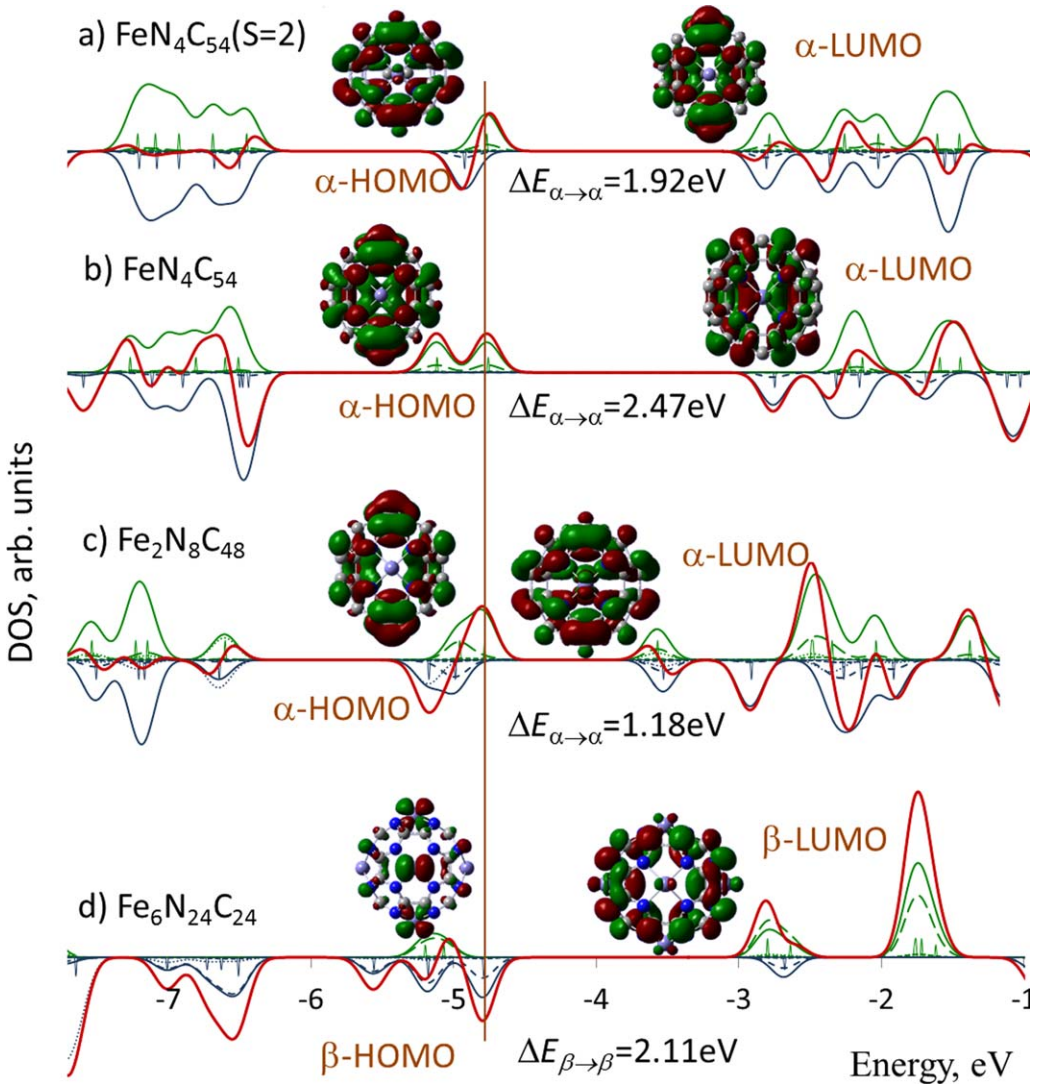

Figure 2. Density of states of Fe-derived nanoclusters. The DOS(α)-DOS(β) spin polarization is presented by red line. Spin-up and spin-down total and partial DOSes of (a) FeN_4C_{54} ($S = 1$); (b) FeN_4C_{54}; (c) $Fe_2N_8C_{48}$; (d) $Fe_6N_{24}C_{24}$ nanoclusters are presented in green (α TDOS) and blue (β TDOS). The partial $|p_C\rangle$, $|p_N\rangle$, and $|d_{Fe}\rangle$ are presented as solid $|p_C\rangle$, long dashed $|p_N\rangle$, and dotted $|d_{Fe}\rangle$ curves, respectively. Short vertical lines represent the MO energy levels. Visualizations of HOMO and LUMO are presented as well. More details of numerical analyses of MO structure in wide energy range are presented in Tables (2–5).

1.6 kcal/mol ($\Delta E[FeN_4C_{54}(S=1)]_{C_{2v}} = 0.0$, $\Delta E[FeN_4C_{54}(S=1)]_{C_1} = 1.6$, $\Delta E[FeN_4C_{54})_{C_{2v}} = 1.2$, $\Delta E[FeN_4C_{54})_{C_1} = 1.2$ kcal/mol) that is close to accuracy (~1 kcal/mol) of both MPWB95 and M06 DFT potentials.[22–25]

The HOMO → LUMO splitting $\Delta E_{\alpha \to \alpha}$ of $FeN_4C_{54}(S = 1)$ is equal to 1.92 eV whereas $\Delta E_{\beta \to \beta} = 2.05$eV and E(α-HOMO) is −4.96 eV against lower E(β-HOMO) = −5.11 eV. HOMOs and LUMOs of both α and β spins are formed by $|p_C\rangle$ (82–85%)

Table 2. AOs contribution to forming MOs of $Fe_6N_{24}C_{24}$, %.

α-MO	E (eV)	$\|p_C\rangle$	$\|p_N\rangle$	$\|d_{Fe}\rangle$	β-MO	E (eV)	$\|p_C\rangle$	$\|p_N\rangle$	$\|d_{Fe}\rangle$
L+4	−1.76	65	30	0	L+4	0.1	71	5	21
L+3	−1.77	51	44	3	L+3	0.1	71	5	21
L+2	−2.64	38	56	4	L+2	−0.34	78	6	12
L+1	−2.8	41	53	4	L+1	−0.9	46	46	0
LUMO	−2.8	41	53	4	LUMO	−2.68	63	34	0
HOMO	−5.07	51	43	1	HOMO	−4.79	64	33	0
H-1	−5.2	54	40	1	H-1	−4.79	64	33	0
H-2	−7.83	13	55	31	H-2	−5.18	53	41	4
H-3	−7.98	11	54	33	H-3	−5.18	53	41	4
H-4	−7.98	11	54	33	H-4	−5.56	50	44	4

Table 3. AOs contribution to forming MOs of FeN_4C_{54} ($S = 1$), %.

α-MO	E (eV)	$\|p_C\rangle$	$\|p_N\rangle$	$\|d_{Fe}\rangle$	β-MO	E (eV)	$\|p_C\rangle$	$\|p_N\rangle$	$\|d_{Fe}\rangle$
L+4	−1.75	96	3	0	L+4	−1.78	95	2	1
L+3	−1.90	97	2	0	L+3	−1.85	96	2	0
L+2	−2.30	80	17	0	L+2	−2.30	81	16	0
L+1	−2.53	90	7	0	L+1	−2.63	90	5	2
LUMO	−3.04	85	13	0	LUMO	−3.06	84	14	0
HOMO	−4.96	82	14	1	HOMO	−5.11	83	13	2
H-1	−6.59	91	6	1	H-1	−6.64	93	5	0
H-2	−6.82	97	1	0	H-2	−6.81	97	1	0
H-3	−7.05	97	1	0	H-3	−7.05	97	1	0
H-4	−7.21	94	4	0	H-4	−7.20	94	4	0

Table 4. AOs contribution to forming MOs of FeN_4C_{54}, (S = 2) %.

α-MO	*E* (eV)	$\|p_C\rangle$	$\|p_N\rangle$	$\|d_{Fe}\rangle$	β-MO	*E* (eV)	$\|p_C\rangle$	$\|p_N\rangle$	$\|d_{Fe}\rangle$
L+4	−1.15	92	6	0	L+4	−1.55	93	4	1
L+3	−1.87	96	2	0	L+3	−2.1	70	27	0
L+2	−2.01	97	1	0	L+2	−2.56	91	5	2
L+1	−2.54	88	9	0	L+1	−2.72	95	2	0
LUMO	−2.63	92	5	0	LUMO	−3.14	84	12	2
HOMO	−5.1	78	20	0	HOMO	−6.74	91	6	1
H-1	−5.45	79	18	1	H-1	−6.78	98	1	0
H-2	−6.81	92	5	1	H-2	−6.8	98	1	0
H-3	−6.9	99	0	0	H-3	−7.19	93	5	0
H-4	−7.1	96	3	0	H-4	−7.4	88	5	5

and $|p_N\rangle$ (13–14%), respectively, according to the partial DOS (Fig. 2a and Table 3). Similarly, the spin-polarized orbitals of third vacant MOs (L+2) orbital consist of $|p_C\rangle$ (80 and 81%) with admixture of $|p_N\rangle$ (17 and 16%), respectively. The rest of the MOs near the HOMO-LUMO region in the Table 3 are formed exclusively by *p* AOs of carbon atoms. Spin polarization occurs due to a slight shift in energy of α and β MO structures.

As considered earlier, the total energies of FeN_4C_{54} of both $S = 1$ and $S = 2$ spin states are almost equal and both states should be described. One can observe again that MOs near the HOMO-LUMO region mostly consist of carbon AOs $|p_C\rangle$ with 20% $|p_N\rangle$ contributions in α-HOMO, 18% in α-H-1, 12% in β-LUMO, and 27% in β-L+3, respectively (Fig. 2b and Table 4). Different weights of carbon and nitrogen *p*-AOs in α and β MOs lead to spin splitting. A splitting $\Delta E_{\alpha \rightarrow \alpha} = 2.47$ eV between vacant and occupied MOs of FeN_4C_{54} is much wider than the α-HOMO → LUMO splitting in FeN_4C_{54} ($S = 1$), with $\Delta E_{\beta \rightarrow \beta} = 3.60$eV of FeN_4C_{54} the widest one. *E*(α-HOMO) is −5.10 eV and *E*(β-HOMO) = −6.74 eV that mainly provides significant difference between the α and β splittings with increasing multiplicity from triplet ($S = 1$) to pentet ($S = 2$) states which causes higher spin polarization of the FeN_4C_{54} nanocluster.

The pentet ground state of $Fe_2N_8C_{48}$ is the lowest in energy with triplet state higher in energy by 5.4 kcal/mol. The relative energy (12 kcal/mol) of triplet state of $Fe_6N_{24}C_{24}$ clearly shows the key role of Fe–Fe interactions in determination of spin states of $(FeN_4)_nC_{6(10-n)}$ nanoclusters. Larger contribution of the Fe *d*-AOs in $Fe_2N_8C_{48}$ is observed in comparison with the FeN_4C_{54} of both multiplicities (Fig. 2d, Table 5). Orbitals in HOMO-LUMO region of $Fe_2N_8C_{48}$ mostly consist of $|p_C\rangle$ with visible admixture of $|p_N\rangle$ but contribution of $|d_{Fe}\rangle$ to LUMOs (14 and 13%) and L+2 (11 and 23%) is significant for both spin orientations and β H-4 (17%) as well. The $|d_{Fe}\rangle$ AOs are vastly responsible for the formation of α H-2 (45%) as well as for both β H-1 (48%) and H-2 (56%) and turn to be competitive with the dominant carbon *p*-AOs, whereas influence of nitrogen AOs is vanished (2–3%). Hence, spin polarization is caused due to the difference in contributions of carbon and nitrogen *p*-AOs as well as iron *d*-AOs. The HOMO → LUMO splitting $\Delta E_{\alpha \rightarrow \alpha} = 1.18$ eV is close to $\Delta E_{\beta \rightarrow \beta} = 1.42$ eV (*E*(α-HOMO) = −4.51eV and *E*(β-HOMO) = −4.71eV, Fig. 2c).

Table 5. AOs contribution to forming MOs of $Fe_2N_8C_{48}$, %.

α-MO	*E* (eV)	$\|p_C\rangle$	$\|p_N\rangle$	$\|d_{Fe}\rangle$	β-MO	*E* (eV)	$\|p_C\rangle$	$\|p_N\rangle$	$\|d_{Fe}\rangle$
L+4	−1.84	89	8	1	L+4	−1.94	90	8	0
L+3	−2.14	73	24	0	L+3	−2.06	73	24	0
L+2	−2.27	68	19	11	L+2	−2.14	61	14	23
L+1	−2.28	77	18	2	L+1	−2.69	93	5	0
LUMO	−3.33	62	22	14	LUMO	−3.29	64	21	13
HOMO	−4.51	92	6	0	HOMO	−4.71	63	34	0
H-1	−4.68	61	36	0	H-1	−4.89	48	3	48
H-2	−6.28	52	2	45	H-2	−6.32	40	3	56
H-3	−6.81	76	14	9	H-3	−6.83	99	0	0
H-4	−6.89	99	0	0	H-4	−6.87	75	7	17

To study energy of formation of the nanoclusters, the following chemical reactions of substitution of C_6 fragments by MN_4 units (Fig. 1) are considered:

$$C_{60} + 2nN_2 + nM = (MN_4)_nC_{6(10-n)} + 3nC_2$$

The energies of formation are calculated using the DFT 6-31G(d)/6-311G(d) total energies of $(MN_4)_nC_{6(10-n)}$ nanoclusters, C_{60}, C_2, and N_2 molecules and M atoms and taking into account the BSSE corrections by placing the atomic orbital basis sets of the moieties on distance 20 Å from each other as vertexes of a pyramid.

For the Fe-derived clusters, the following formation energies are: $\Delta E(FeN_4C_{54}) = 11.2$ kcal/mol/atom, $\Delta E(Fe_2N_8C_{48}) = 23.5$ kcal/mol/atom (or 11.8 kcal/mol/atom per one Fe ion), and $\Delta E(Fe_6N_{24}C_{24}) = 71.4$ kcal/mol/atom (or 11.9 kcal/mol/atom per one Fe ion). The triplet and pentet states of FeN_4C_{54} have almost the same formation energies (11.25 against 11.19 kcal/mol/atom). One can see the formation energy of the Fe-substituted clusters depends linearly on the number of FeN_4 fragments to be inserted in the carbon lattice of the fullerene.

Formation energies of Mg- and Zn-substituted clusters are equal to $\Delta E(Mg_6N_{24}C_{24}) = 70.4$ kcal/mol/atom (11.7 kcal/mol/atom per Mg ion) and $\Delta E(Zn_6N_{24}C_{24}) = 76.5$ kcal/mol/atom (12.8 kcal/mol/atom per Zn ion). The sixfold-substituted nanoclusters demonstrate slight increase of the formation energy per one metal ion with the increasing of the atomic number from Mg to Zn and increasing of the formation energy upon increasing of atomic radius of the metals (the atomic radii of Mg, Fe, and Zn are 1.50, 1.40, and 1.35 Å, respectively). To prove the stability of the nanoclusters, the energy of extraction of magnesium ion atom from MgN_4C_{54} also was calculated at M06/6-311G(d)/6-31G(d) level of theory. It was found that it is very endothermic and equal to −116.3 kcal/mol (−2.0 kcal/mol/atom) that proves high energetic stability of the nanoclusters.

Conclusion

Hollow-caged fullerene-derived nanoclusters with metal ions inserted in the carbon lattice by substitution of C_6 hexagons by MN_4 fragments were introduced and studied by LC DFT technique in cluster approximation. At MPWB95 and partially M06 levels of theory with 6-31G/6-311G(d) basis sets, the energy cost of formation of $(MN_4)_nC_{6(10-n)}$ systems from C_{60} is

endothermic in the range of 11.7–12.8 kcal/mol/atom. It is found that the energy cost of substitution linearly increases with increasing of the numbers of incorporated metal ions. Fragments centered on metallic units were shown to be quite stable in the studied structures. The antiaromaticity of the MN_4C_{20} structural units causes significant decrease in the structural stress and energy stabilization of the proposed closed-shell nanoclusters. For the Fe-derived nanoclusters, the HOMO-LUMO energy region mostly consists of carbon and nitrogen *p*-AOs with an admixture of iron *d*-AOs which depends on number of iron centers. Unique magnetic properties of Fe-based molecules are caused by strong spin polarization formed by the significant difference between contributions of these AOs to α and β MOs. High spin states and correlated electronic structure of the clusters allows one to use Fe-derived structures as molecular supermagnets and heterogenic catalysis.

Acknowledgment

All calculations were carried out on the Computational Center of Tomsk State University "SKIF."

Keywords: C_{60} fullerene · porphyrins · electronic structures · - spin-polarization · formation energy

How to cite this article: V. A. Pomogaev, P. V. Avramov, A. A. Kuzubov, V. Y. Artyukhov. *Int. J. Quantum Chem.* **2015**, *115*, 239–244. DOI: 10.1002/qua.24840

Additional Supporting Information may be found in the online version of this article.

[1] H. W. Kroto, J. R. Heath, S. C. Obrien, R. F. Curl, R. E. Smalley, *Nature* **1985**, *318*, 162.
[2] D. A. Bochvar, E. G. Gal'pern, *Proc. Acad. Sci. USSR* **1973**, *209*, 239.
[3] H.-J. Muhr, R. Nesper, B. Schnyder, R. Kötz, *Chem. Phys.Lett.* **1996**, *249*, 399.
[4] J. C. Hummelen, B. Knight, J. Pavlovich, R. González, F. Wud, *Science* **1995**, *269*, 1554.
[5] M. Saunders, H. A. Jimenez-Vazquez, R. J. Cross, R. J. Poreda, *Science* **1993**, *259*, 1428.
[6] J. Schnadt, P. A. Brühwiler, N. Mårtensson, A. Lassesson, F. Rohmund, E. E. B. Campbell, *Phys. Rev. B* **2000**, *62*, 4253.
[7] Y. Chai, T. Guo, C. Jin, R. E. Haufler, L. P. F. Chibante, J. Fure, L. Wang, J. M. Alford, R. E. Smalley, *J. Phys. Chem.* **1991**, *95*, 7564.
[8] J. R. Heath, S. C. O'Brien, Q. Zhang, Y. Liu, R. F. Curl, H. W. Kroto, F. K. Tittel, R. E. Smalley, *J. Am. Chem. Soc.* **1985**, *107*, 7779.
[9] D. H. Lee, W. J. Lee, S. O. Kim, Y.-H. Kim, *Phys. Rev. Lett.* **2011**, *106*, 175502.
[10] E. Hückel, Z. Physik. **1931**, *70*, 204.
[11] V. I. Minkin, *Pure Appl. Chem.* **1999**, *71*, 1919.
[12] A. Tsuda, H. Furuta, A. Osuka, *Angew. Chem. Int. Ed. Engl.* **2000**, *39*, 2549.
[13] N. Aratani, A. Osuka, H. S. Chob, D. Kimb, *J. Photochem. Photobiol. C* **2002**, *3*, 25.
[14] K. S. Kim, J. M. Lim, A. Osuka, D. Kim, *J. Photochem. Photobiol. C* **2008**, *9*, 13.
[15] T. Tanaka, B. S. Lee, N. Aratani, M.-C. Yoon, D. Kim, A. Osuka, *Chem. Eur. J.* **2011**, *17*, 14400.
[16] S. Tanaka, T. Sakurai, Y. Honsho, A. Saeki, S. Seki, K. Kato, M. Takata, A. Osuka, T. Aida, *Chem. Eur. J.* **2012**, *18*, 10554.
[17] Y. Nakamura, N. Aratani, H. Shinokubo, A. Takagi, T. Kawai, T. Matsumoto, Z. S. Yoon, D. Y. Kim, T. K. Ahn, D. Kim, A. Muranaka, N. Kobayashi, A. Osuka, *J. Am. Chem. Soc.* **2006**, *128*, 4119.
[18] T. Miyahara, H. Nakatsuji, J. Hasegawa, A. Osuka, N. Aratani, A. Tsuda, *J. Chem. Phys.* **2002**, *117*, 11196.
[19] H. Nakanishi, K. Miyamoto, M. Y. David, E. S. Dy, R. Tanaka, H. Kasai, *J. Phys.: Condens. Matter* **2007**, *19*, 365234.
[20] K. Nakai, K. Kurotobi, A. Osuka, M. Uchiyama, N. Kobayashi, *J. Inorg. Biochem.* **2008**, *102*, 466.
[21] S. Ohmori, H. Kawabata, K. Tokunaga, H. Tachikawa, *Thin Solid Films* **2009**, *518*, 901.
[22] V. Pavel, P. V. Avramov, A. A. Kuzubov, S. Sakai, M. Ohtomo, S. Entani, Y. Matsumoto, S. Natalia, N. S. Eleseeva, V. A. Pomogaev H. Naramoto, *J. Porphyrins Phthalocyanines* **2014**, *18*, 552.
[23] E. Ali Md, B. Sanyal, P. M. Oppeneer, *J. Phys. Chem. B* **2012**, *116*, 5849.
[24] Y. Zhao, D. Truhlar, *Theor. Chem. Acc.* **2008**, *120*, 215.
[25] C. Adamo, V. Barone, *J. Chem. Phys.* **1998**, *108*, 664.
[26] J. R. Sabin, E. J. Brandas, Advances in Quantum Chemistry: Theory of Confined Quantum Systems - Part Two, Vol. *58*; Academic Press, **2009**.
[27] M. J. Frisch, G. W. Trucks, H. B. Schlegel, G. E. Scuseria, M. A. Robb, J. R. Cheeseman, J. A. Montgomery, T. Vreven, K. N. Kudin, J. C. Burant, J. M. Millam, S. S. Iyengar, J. Tomasi, V. Barone, B. Mennucci, M. Cossi, G. Scalmani, N. Rega, G. A. Petersson, H. Nakatsuji, M. Hada, M. Ehara, K. Toyota, R. Fukuda, J. Hasegawa, M. Ishida, T. Nakajima, Y. Honda, O. Kitao, H. Nakai, M. Klene, X. Li, J. E. Knox, H. P. Hratchian, J. B. Cross, V. Bakken, C. Adamo, J. Jaramillo, R. Gomperts, R. E. Stratmann, O. Yazyev, A. J. Austin, R. Cammi, C. Pomelli, J. W. Ochterski, P. Y. Ayala, K. Morokuma, G. A. Voth, P. Salvador, J. J. Dannenberg, V. G. Zakrzewski, S. Dapprich, A. D. Daniels, M. C. Strain, O. Farkas, D. K. Malick, A. D. Rabuck, K. Raghavachari, J. B. Foresman, J. V. Ortiz, Q. Cui, A. G. Baboul, S. Clifford, J. Cioslowski, B. B. Stefanov, G. Liu, A. Liashenko, P. Piskorz, I. Komaromi, R. L. Martin, D. J. Fox, T. Keith, M. A. Al-Laham, C. Y. Peng, A. Nanayakkara, M. Challacombe, P. M. W. Gill, B. Johnson, W. Chen, M. W. Wong, C. Gonzalez, J. A. Pople, Gaussian 09; Gaussian, Inc.: Wallingford, CT, **2009**.
[28] J. Lu, X. Zhang, X. Zhao, *Appl. Phys. A* **2000**, *70*, 461.
[29] E. Broclawik, A. Eilmes, *J. Chem. Phys.* **1998**, *108*, 3498.
[30] M.-H. Liao, J. D. Watts, M.-J. Huang, *J. Phys. Chem. B* **2007**, *111*, 4374.
[31] V. A. Basiuk, *J. Phys. Chem. A* **2005**, *109*, 3704.
[32] M.-H. Liao, J. D. Watts, M.-J. Huang, *Chem. Phys.* **2009**, *11*, 4365.
[33] P. F. Weck, E. Kim, K. R. Czerwinski, D. Tománek, *Phys. Rev. B* **2010**, *81*, 125448.
[34] L. J. Jing, X. Zhang, X. Zhao, *Solid State Commun.* **1999**, *110*, 565.
[35] S. F. Boys, F. Bernardi, *Mol. Phys.* **1970**, *19*, 553.
[36] N. O'boyle, A. Tenderholt, K. J. Langner, *Comput. Chem.* **2008**, *29*, 839.

Received: 23 September 2014
Revised: 11 November 2014
Accepted: 18 November 2014
Published online 28 November 2014